2018

Theoretical Model For Buoyancy-Induced Heat Transfer Deterioration Under Supercritical Pressure

Jiacheng He
the University of Tokyo, Japan, palmhe@hee.k.u-tokyo.ac.jp

Chaobin Dang
dangcb@k.u-tokyo.ac.jp

Eiji Hihara
The university of Tokyo, Japan, hihara@k.u-tokyo.ac.jp

Theoretical Model for Buoyancy-Induced Heat Transfer Deterioration Under Supercritical Pressure

Jiacheng HE*, Chaobin DANG, Eiji HIHARA

The University of Tokyo, Department of Human and Engineered Environmental Studies,
Graduate school of frontier sciences,
Kashiwa, Chiba, Japan
+81-4-7136-4630, palmhe@hee.k.u-tokyo.ac.jp

* Corresponding author

ABSTRACT

Through analysis of the experimental results of buoyancy-induced heat transfer deterioration at supercritical conditions, a theoretical model based on the force equilibrium is developed for the vertically upward supercritical flow under heating conditions. A program code is designed to simulate the effect of buoyancy on the degree of heat transfer deterioration. The simulation results for a wall temperature of 175℃ are presented. They show that the salient point in the M-shaped velocity profile plays a key role in heat transfer deterioration. The salient point locates at low y^+ when the deterioration occurs, and it moves to higher y^+ as the friction Reynolds number increases. Furthermore, the salient points will consistently locate behind the pseudocritical point in the boundary. Heat transfer will recover when the condition of force equilibrium is not met, manifested by bulk fluid temperature that is slightly lower than the pseudocritical temperature.

1. INTRODUCTION

In various applications, including light water reactors and organic Rankine cycles, supercritical fluids are widely used as the working fluid in consideration of the system efficiency or compactness. In a recent study, the authors performed an experiment with a working fluid of R245fa and R1233zd(E) in a vertical tube with an inner diameter of 4 mm and length of 1.04 m. Some experimental results are shown in Figures 1 to 3. For R245fa, the normal heat transfer was observed under low heat flux, as shown in Figure 1, which is consistent with the previous experimental results. The maximum heat transfer coefficient existed in the regions where the local bulk fluid temperature was close to the pseudocritical temperature, and it decreased in magnitude with pressure. The heat transfer deterioration was obtained when the heat fluxes increased, as shown in Figure 2. A significant drop in the heat transfer coefficient occurred at the illustrated heat flux under all the investigated pressures. The wall temperature was higher than the pseudocritical temperature when the deterioration occurred, whereas the bulk fluid temperature was less than it. The heat transfer showed recovery when the bulk fluid temperature approached the pseudocritical temperature. In Figure 3, comparison of the experimental results between R245fa and R1233zd(E) is presented under a reduced pressure of 1.1, which was 4 MPa for R245fa and 3.93 MPa for R1233zd(E). In the figure, the heat transfer coefficient for R1233zd(E) shows monotonic change with bulk fluid temperature, whereas deterioration occurred for R245fa. Such a heat transfer characteristic is unusual, because the heat transfer deterioration would take place at certain working conditions for a number of working fluids.

Some common features can be summarized from the experimental investigations. When the bulk fluid temperature is much lower than the pseudocritical temperature, the heat transfer coefficient shows similar characteristics to those of the fluid under subcritical pressures. As the bulk fluid temperature approaches the pseudocritical temperature, it increases monotonically and takes a maximum when the bulk temperature is slightly less than the pseudocritical temperature under the conditions with low heat fluxes. The vapor like fluid appears to dominate the heat transfer, which leads to a lower heat transfer coefficient when the bulk fluid temperature is high enough. As the heat flux increases, the maximum heat transfer coefficient observed near the pseudocritical point is suppressed. At a moderate heat flux, heat transfer deterioration takes place, which is manifested as a sudden increase in wall temperature. Such a heat transfer only occurs when the bulk fluid temperature is less than the pseudocritical temperature, whereas the

wall temperature exceeds it. In addition, as obtained in various experimental investigations (Bae *et al*., 2010 and 2011), the experimental pressures have little influence on heat transfer deterioration. The heat transfer will recover as the bulk fluid temperature increases to a value that is slightly lower than the pseudocritical temperature, characterized by a decrease in wall temperature. As a result, the heat transfer deterioration can occur under the same wall temperature and different fluid temperatures.

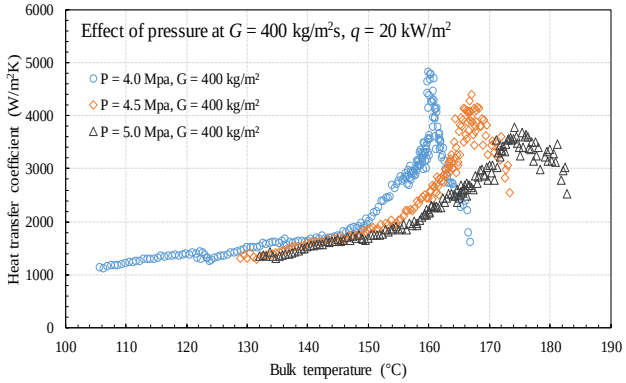

Figure 1. Heat transfer characteristics of R245fa for low heat flux

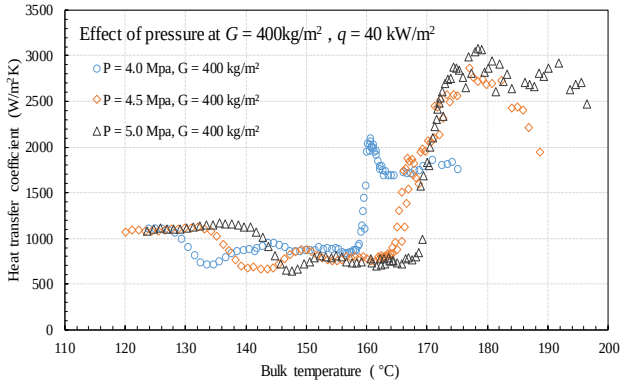

Figure 2. Heat transfer deterioration under moderate heat flux

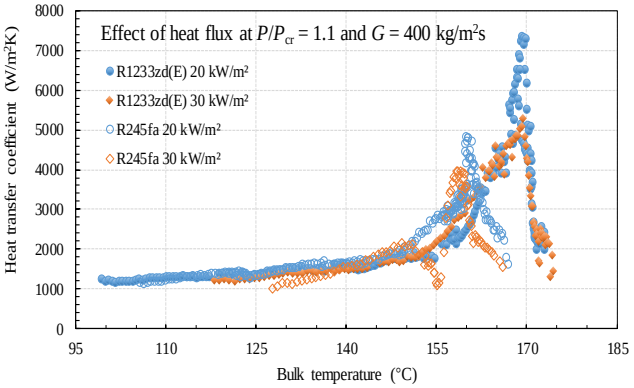

Figure 3. Comparison of the experimental results between R245fa and R1233zd(E)

In general, the heat transfer of a supercritical working fluid shows distinct characteristics under different heat fluxes. The heat transfer deterioration usually occurs at a moderate heat flux, characterized by a significant increase in the wall temperature. Surprisingly, such deterioration did not occur in the experimental study of the lately developed R1233zd(E), which motivates exploration for a better understanding of the underlying mechanism behind the

supercritical heat transfer. In this study, to further understand buoyancy-induced heat transfer deterioration, a theoretical analysis based on the local force equilibrium is presented, including the force analysis, the details of simulation, and discussion of the simulation results.

2. THE PROPOSED MECHANISM

2.1 Consideration of Heat Transfer Deterioration

In a fully developed turbulent flow, it is generally recognized that the peak kinetic energy is produced within the viscous buffer layer inside the boundary at a dimensionless wall distance y^+ of approximately 12 (Li *et al*., 2004; Marusic *et al*., 2010; Smits *et al*., 2011). However, at high Reynolds numbers, the major contribution to the bulk turbulence production comes from the logarithmic region (Smits *et al*., 2011).

For heat transfer under supercritical pressure, the inlet Reynolds number is on the order of approximately 1E+04, and it reaches a greater value when the fluid temperature crosses the critical point. As a result, the friction Reynolds number increases as well, even though the linear relation between the friction Reynolds and the Reynolds number defined by the bulk fluid velocity is not valid. Thus, as the fluid is heated continuously until the bulk temperature approaches the pseudocritical temperature, the friction Reynolds numbers increase consequently, and the contribution to the turbulent kinetic energy production is increasingly dominated by the region with higher y^+.

The M-shaped velocity profile which is formed with the significant drop in density, accompanies both the heat transfer deterioration and the recovery process. The flow is either turbulent or laminar, which might depend on the slope of the velocity profile, resulting in the occurrence of heat transfer deterioration. Some relevant information (Kurganov *et al*., 1992; Tanaka *et al*., 1987) can be found in other publications. From these velocity profiles with various slopes, a characteristic emerges that salient points that are the climax in the velocity appear in different locations. Because the local shear stresses at these salient points equals zero, it is reasonable to relate the flow state, i.e., turbulent flow or laminar flow, to the slope of the velocity profile or, more illustratively, the location of the salient point.

A force analysis was carried out on the narrow fluid layer between the wall surface and salient point of the velocity profile. As shown in Figure 4, the blue dotted line represents the M-shaped velocity profile at a certain cross-section. The wall shear stress acts on left edge of the narrow layer, and the buoyancy acts on the whole bulk fluid layer. Given that the local shear stress on the right edge equals zero, the wall shear stress and the buoyancy balance each other; thus, a force equilibrium is achieved. With the varied local temperature profile, the magnitude of buoyancy effect that results from radial gradients in density accordingly varies with the heat transfer condition; consequently, the force equilibrium condition is satisfied on the narrow layer with different thicknesses.

For a fully developed turbulent pipe flow, a velocity profile is yielded that is much flatter across the core of the flow, and this can be approximated quite well with a power law of the form

$$u/u_{\max} = (1 - y/R)^{1/n} \tag{1}$$

The index n is around 7 and referred to as the 1/7 Power Law. This power law gives a good general description of the shape of the turbulent core velocity profile, even though it fails in regions very close to the wall.

As with velocity, the temperature profile under a heating condition with constant heat flux also follows the 1/7 Power Law:

$$(t_w - t)/(t_w - t_c) = (1 - y/R)^{1/7} \tag{2}$$

Under supercritical pressures, by contact, the flow is significantly affected by buoyancy, and, thus, the M-shaped velocity profile exists; as a result, the power law is not able to describe the shape of the velocity profile. However, unlike the velocity, the temperature shows a monotonic profile in the radial direction (You *et al*., 2003; Keshmiri *et al*., 2016) either in Reynolds averaged Navier–Stokes (RANS) or direct numerical simulation (DNS) studies, indicating that the power law is still able to describe the temperature variation at the cross sections.

2.2 Development of the model and details of the simulation

Based on the above analysis, a theoretical approach is presented to model quantitatively the heat transfer deterioration caused by buoyancy under supercritical pressures.

The buoyancy resulting from the radial density gradient is

$$F_B = \int_0^{\delta_B} (\rho_B - \rho_i) g dy \tag{3}$$

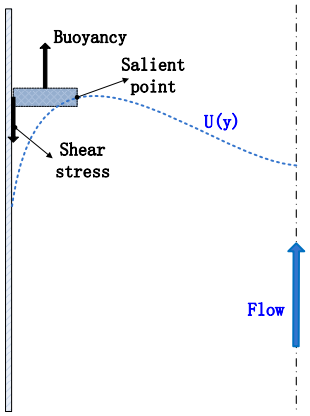

Figure 4. Local force analysis

where ρ_B and ρ_i represent the bulk fluid density and local density, respectively, δ_B stands for the thickness of the thin layer in Figure 4, and g is the acceleration of gravity.
The wall shear stress can be related to pressure drop along the pipe with the following equation:

$$\tau_w = -\frac{d}{4}\frac{dP}{dx} \tag{4}$$

In the pipe flow, the pressure drop consists of static pressure drop, acceleration pressure drop, and friction pressure drop. In such a thin analysis object in Figure 4, the static pressure drop and acceleration pressure drop can be neglected because of the negligible density change. For the friction pressure drop, several experimental studies regarded it as a modified pressure drop of single phase flow with consideration of the thermophysical properties' effect in the pseudocritical region. In those studies, the friction pressure drop decreased when the bulk fluid temperature was close to the pseudocritical temperature (Yamashita *et al*., 2003). A summary of the pressure drop correlations can be found in the reviews of research (Cheng *et al*., 2001; Cheng *et al*., 2008). Because these correlations were developed with certain working fluids, the magnitudes of variation in thermophysical properties might differ, so the correlation shown as Equation (7) is adopted in this study because of the lack of pressure drop measurement results.

$$\frac{dP}{dx} = f\frac{G^2}{2\rho_B}\frac{1}{d} \tag{5}$$

$$\tau_w = -\frac{f}{4}\frac{G^2}{2\rho_B} \tag{6}$$

$$f = (1.82\log(Re_b/8))^{-2}\left(\frac{\rho_w}{\rho_B}\right)^{0.4} \tag{7}$$

To obtain the buoyancy force, the local fluid temperature in the cross-section is necessary. The power law is used for local temperature to provide the temperature distribution in the radial direction. For a turbulent pipe flow under heating conditions, the supplied heat is transported through both the molecular diffusion and the turbulent diffusion. Generally, the molecular diffusion is dominant in a viscous sublayer inside the boundary layer, while the turbulent diffusion dominates in the log-law region and beyond. In heat transfer deterioration conditions, the transportation of heat is suppressed the most if the salient point locates in the region that dominates the contribution to the turbulent kinetic energy production, which is manifested as a local maximum dimensionless temperature at such a position. The turbulent diffusion has a dominant effect behind the buffer layer, and the shear stress that contributes to the turbulent diffusion also equals zero under deterioration conditions. Thus, the salient point in the velocity profile and the maximum (dimensionless) temperature coincide.

A program code is used to model the process. The flowchart is shown in Figure 5. The modeling details are explained as follows.

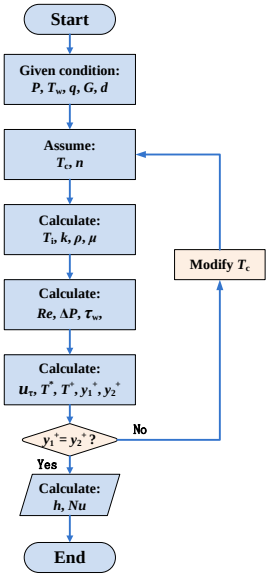

Figure 5. Flowchart of the simulation

For a given condition with heat flux, mass flux, and wall temperature, a centerline temperature T_c and n, the index of the power law equation, are assumed. A temperature profile, therefore, can be calculated by the power law with these parameters. The local thermal physical properties can also be calculated consequently. The whole cross section is divided into 50,000 subsections, and the local buoyancy for each subsection can be calculated with Equation (3). Adding up the local buoyancies, the summary of buoyancy that equals wall shear stress at a certain distance from the wall is denoted as y_1. However, the local dimensionless temperature is calculated as

$$T_i^+ = \frac{T_w - T_i}{T_{\tau,i}} \tag{8}$$

where

$$T_{\tau,i} = q/\rho_i c_{P,i} u_{\tau,i} \tag{9}$$

and the local friction velocity is calculated with

$$u_{\tau,i} = \sqrt{\tau_w/\rho_i} \tag{10}$$

The maximum dimensionless temperature can be easily found among the calculated T_i^+. The distance from the wall in which dimensionless temperature is maximal is denoted as Y_2. For a given index n, the centerline temperature changes until Y_1 coincides with Y_2. By varying the index, a series of (T_c, n) (or (T_B, n)) is expected to be obtained.
In the simulation, the deterioration condition for R245fa obtained in the experiment is chosen as the given condition. Several selected wall temperatures are adopted as the initial conditions as well. The simulation conditions are summarized in Table 1.

Table 1. Simulation conditions

Working fluid	***P*, MPa**	***q*, kW/m^2**	***G*, kg/m^{2}s**	***d*, mm**	***T*$_w$, °C**
R245fa	4	30	400	4	175, 180, 185, 190, 195

3. RESULTS AND DISCUSSION

In this section, the simulation results are presented. Only the simulation results with wall temperature of 175℃ are discussed for brevity. Then, the validation with experimental data is presented.

3.1 Case of T_w = 175℃

Figure 6 shows the variation in the bulk fluid temperature and Nusselt number ratio with *n* at a wall temperature of 175℃. The bulk temperature is calculated by averaging all the local fluid temperatures, and the Nusselt number ratio is defined as the ratio between the calculated Nusselt number and the Nusselt number obtained by the Dittus–Boelter equation.

The initial value of *n* is 4.5, and the corresponding bulk fluid temperature is 143.06℃ when the forces' balance condition is satisfied. Figure 6 shows that the index *n* changes with a small interval to obtain the onset of deterioration. Under the illustrated condition, the onset of the deterioration indicated by the decrease in the Nusselt number ratio occurs with an index of 5.

Figure 7 shows the variation in Reynolds number (*Re*) and friction Reynolds number (Re_τ) with the index *n*. The Reynolds number is defined with bulk fluid velocity, whereas the friction Reynolds number is defined with the friction velocity U_τ. The Re and Re_τ increase monotonously with the index *n*, implying that the viscosity of the fluid is decreasing. Given that the bulk fluid temperature increases with the index *n*, the variation in the Reynolds numbers agrees with the variation in the bulk temperature.

In summary, with a given wall temperature, the variation in the index *n* is capable of reproducing the variation in the bulk fluid temperature, and the Nusselt number ratio can be obtained; thus, the buoyancy-induced heat transfer deterioration can be reproduced.

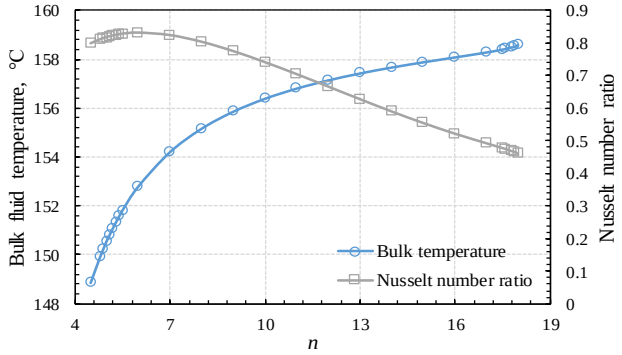

Figure 6. Variation in bulk fluid temperature and Nusselt number

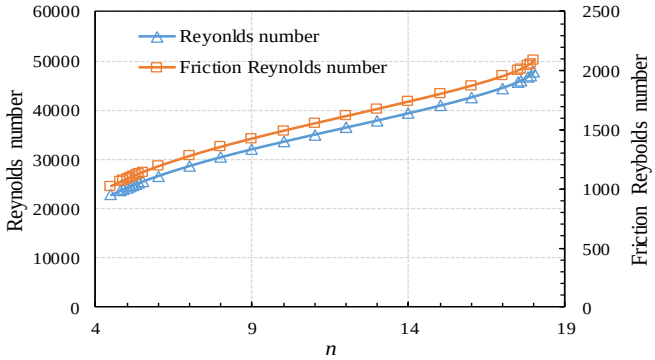

Figure 7. Variation in Reynolds number and friction Reynolds number

3.2 Comparison with Experimental Data of R245fa

To obtain a clearer picture of the buoyancy-induced heat transfer deterioration, the variations in the location of the salient points and pseudocritical points as well as the Nusselt number ratio with Re_τ are shown in Figure 8. The salient point represents the maximum in the velocity and temperature profiles. The dimensionless distance y^+ is used to

identify clearly the exact location in the boundary layer of the salient point as well as the pseudocritical point. y^+ is calculated as

$$y^+ = Yu_{\tau,i}/\upsilon_i \tag{1}$$

In Figure 8, the salient point locates at low y^+ under the condition with small Re_τ, which corresponds to the onset of the deterioration of heat transfer. As the Re_τ increases, the location of the salient point moves to a higher y^+, and the Nusselt number ratio decreases as well. In the simulation, the maximum y^+ exceeds 300, in which the most severe deterioration takes place.

The location of the pseudocritical point, which is defined as the temperature that corresponds to the maximum value of the specific heat capacity for a given pressure, is also illustrated in Figure 9. The salient points locate behind the pseudocritical point under all Re_τ. At small Re_τ, for example, the salient point and pseudocritical point locate at y^+ of 47.35 and 44.6, respectively. As the Re_τ increases, the discrepancy between them is increasingly significant, implying that the salient point in the velocity profile locates increasingly behind the pseudocritical point.

As mentioned in Section 3, the major contribution to the bulk turbulence production comes from the logarithmic region of the boundary layer at high Reynolds numbers (Smits *et al.*, 2011). For the supercritical heat transfer, both the *Re* and Re_τ increase resulted from the change in thermophysical properties; thus, the dominant contribution to the turbulence production comes from the region with higher y^+. The magnitude of the deterioration, which is manifested as the Nusselt number ratio, becomes increasingly significant if the dominant turbulence production is damaged. In Figure 8, the buoyancy-induced heat transfer deterioration starts at a y^+ of 47.35 under a Re_τ of 1085 and ends at a y^+ of more than 300 under a Re_τ of more than 2000. The heat transfer recovers when the salient point locates behind the region that dominates the turbulence production. Such a characteristic agrees with the published result (Kurganov *et al.*, 1992), which showed the variation in M-shaped velocity profiles in the deterioration working condition.

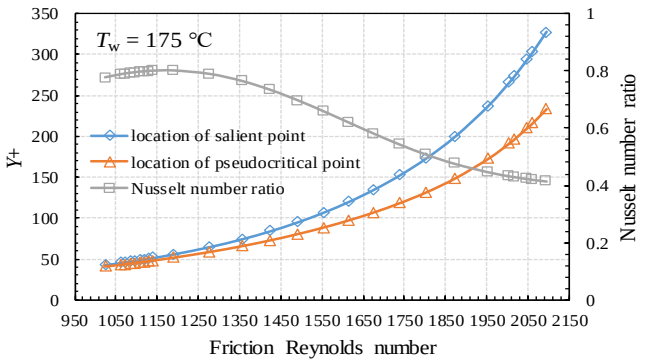

Figure 8. Variation in the location of salient point and pseudocritical point and *Nu* ratio

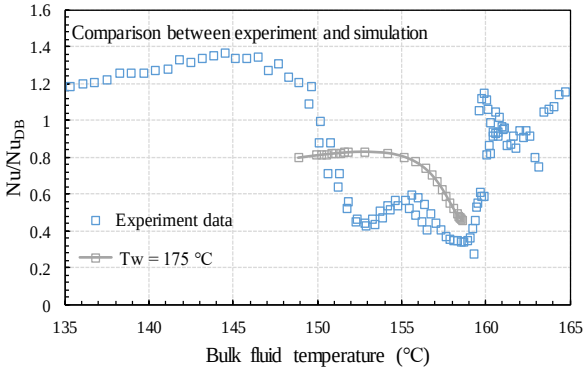

Figure 9. Comparison between experiment and simulation

Figure 9 shows the comparison between the experimental and simulation results. The results from the experiment and simulation are plotted in terms of the Nusselt number ratio and bulk fluid temperature. The buoyancy-induced heat transfer deterioration is clearly expressed by a significant drop in the Nusselt number ratio. For the simulation results,

similar trends were obtained for all the investigated wall temperatures. The buoyancy-induced salient point with local zero shear stress significantly damages the turbulence production, resulting in the heat transfer deterioration manifested by a significant increase in wall temperature. The minimum of the Nusselt number ratio takes place at a bulk fluid temperature close to the pseudocritical temperature, in which the most severe buoyancy occurs.

4. CONCLUSIONS

A theoretical model based on the force balance between buoyancy and wall shear stress was proposed. A program code was designed to model the location variation in the salient point in the M-shaped velocity profile with the magnitude of buoyancy under deterioration conditions. The main conclusions are summarized as follows.

- Increase in the index n leads to increase in the Reynolds number and friction Reynolds number; the location of salient points moves to higher y^+, and the degree of deterioration is aggravated.
- The salient points consistently locate behind the pseudocritical point in the boundary, and the discrepancy between them becomes greater as the friction Reynolds number increases.
- Comparison between the experimental and simulation results shows that the onset of deterioration might occur at $y^+ = 47.35$ and ends at $y^+ > 300$.
- When the bulk fluid temperature increases to slightly lower than the pseudocritical temperature, the force balance condition cannot be met, thus leading to the recovery in heat transfer.

NOMENCLATURE

C_P	specific heat capacity	(kJ/kg·K)
d	diameter	(m)
f	friction factor	(–)
F_B	integrated buoyancy	(Pa)
G	mass flux	(kg/(m^{2}s))
g	gravitational acceleration	(m/s^2)
k	thermal conductivity	(W/(m·K))
n	index of power law	(–)
Nu	Nusselt number	(–)
P	pressure	(MPa)
q	heat flux	(kW/m^2)
$R(r)$	radius	(m)
Re	Reynolds number	(–)
T	temperature	(°C or K)
u	flow velocity	(m/s)
Y	distance from wall	(m)
ρ	density	(kg/m^3)
μ	viscosity	(Pa·s)
τ	shear stress	(Pa)

Subscript

B(b)	bulk properties
c	centerline
cri	critical point
i	local parameter
pc	pseudocritical
w	wall
τ	friction properties or normalized with friction velocity
w	wall

Superscript

+	dimensionless parameter

REFERENCES

Bae, Y., Kim, H., Kang, D. (2010). Forced and mixed convection heat transfer to supercritical CO_2 vertically flowing in a uniformly-heated circular tube. *Exp. Therm. Fluid Sci.*, 34(8), 1295-1308.
Bae, Y., Kim, H., Yoo, T.H. (2011). Effect of a helical wire on mixed convection heat transfer to carbon dioxide in a vertical circular tube at supercritical pressures. *Int. J. Heat Fluid Flow*, 32(1), 340-351.
Li, F., Kawaguchi, Y., Hishida, K. (2004). Investigation on the characteristics of turbulence transport for momentum and heat in a drag-reducing surfactant solution flow. *Phys Fluids*, 16(9), 3281-3295.
Marusic, I., Mathis, R., Hutchins, N. (2010). High Reynolds number effects in wall turbulence. *Int. J. Heat Fluid Flow*, 31 (3) 418-428.
Smits, A.J., McKeon, B.J., Marusic, I. (2011). High-Reynolds number wall turbulence. *Annu. Rev. Fluid Mech.*, 43, 353-375.
Kurganov, V.A., Kaptil'Ny, A.G. (1992). Velocity and enthalpy fields and eddy diffusivities in a heated supercritical fluid flow. *Exp. Therm. Fluid Sci.*, 5(4), 465-478.
Tanaka, H., Maruyama, S., Hatano, S. (1987). Combined forced and natural convection heat transfer for upward flow in a uniformly heated. vertical pipe. *Int. J. Heat Mass Transfer*, 30(1), 165-174.
You, J., Yoo, J.Y., Choi, H. (2003). Direct numerical simulation of heated vertical air flows in fully developed turbulent mixed convection. *Int. J. Heat Mass Transfer*, 46(9), 1613-1627.
Keshmiri, A., Revell, A., Darabkhani, H.G. (2016). Assessment of a common nonlinear eddy-viscosity turbulence model in capturing laminarization in mixed convection flows. *Numer. Heat Transfer A*, 69(2), 146-165.
Cheng, X., Schulenberg, T. (2001). Heat transfer at supercritical pressures: Literature review and application to an HPLWR, FZKA.
Cheng, L., Ribatski, G., Thome, J.R. (2008). Analysis of supercritical CO_2 cooling in macro- and micro-channels, *Int. J. Refrig.*, 31(8), 1301-1316.

ACKNOWLEDGMENT

The authors would gratefully acknowledge the financial support by the New Energy and Industrial Technology Development Organization (NEDO)